

10-2013

Small molecule antagonists of melanopsin-mediated phototransduction

Kenneth A. Jones

Lundbeck Research USA Inc., kenjones120@gmail.com

Megumi Hatori

Salk Institute for Biological Studies

Ludovic S. Mure

Salk Institute for Biological Studies

Jayne R. Bramley


University of Nebraska-Lincoln

Roman Artymyshyn

Lundbeck Research USA Inc.

See next page for additional authors

Follow this and additional works at: <http://digitalcommons.unl.edu/vetscipapers>

 Part of the [Biochemistry, Biophysics, and Structural Biology Commons](#), [Cell and Developmental Biology Commons](#), [Immunology and Infectious Disease Commons](#), [Medical Sciences Commons](#), [Veterinary Microbiology and Immunobiology Commons](#), and the [Veterinary Pathology and Pathobiology Commons](#)

Jones, Kenneth A.; Hatori, Megumi; Mure, Ludovic S.; Bramley, Jayne R.; Artymyshyn, Roman; Hong, Sang-Phyo; Marzabadi, Mohammad; Zhong, Huailing; Sprouse, Jeffrey; Zhu, Quansheng; Hartwick, Andrew T. E.; Sollars, Patricia J.; Pickard, Gary E.; and Panda, Satchidananda, "Small molecule antagonists of melanopsin-mediated phototransduction" (2013). *Papers in Veterinary and Biomedical Science*. 259.

<http://digitalcommons.unl.edu/vetscipapers/259>

Authors

Kenneth A. Jones, Megumi Hatori, Ludovic S. Mure, Jayne R. Bramley, Roman Artymyshyn, Sang-Phyo Hong, Mohammad Marzabadi, Huailing Zhong, Jeffrey Sprouse, Quansheng Zhu, Andrew T. E. Hartwick, Patricia J. Sollars, Gary E. Pickard, and Satchidananda Panda



HHS Public Access

Author manuscript

Nat Chem Biol. Author manuscript; available in PMC 2014 April 01.

Published in final edited form as:

Nat Chem Biol. 2013 October ; 9(10): 630–635. doi:10.1038/nchembio.1333.

Copyright Macmillan, Inc. Used by permission.

Small molecule antagonists of melanopsin-mediated phototransduction

Kenneth A. Jones^{1,*}, Megumi Hatori^{2,*}, Ludovic S. Mure^{2,*}, Jayne R. Bramley³, Roman Artymyshyn¹, Sang-Phyo Hong¹, Mohammad Marzabadi¹, Huailing Zhong¹, Jeffrey Sprouse^{1,5}, Quansheng Zhu², Andrew T.E. Hartwick⁴, Patricia J. Sollars³, Gary E. Pickard^{3,6}, and Satchidananda Panda²

¹Lundbeck Research USA Inc., 215 College Road, Paramus, NJ 07652

²Regulatory Biology Laboratory, Salk Institute for Biological Studies, 10010, North Torrey Pines Road, La Jolla, CA 92037

³School of Veterinary Medicine and Biomedical Sciences, University of Nebraska, Lincoln, NE 68583

⁴College of Optometry, The Ohio State University, Columbus, OH 43210

⁵Cyanaptic LLC, 16 School Street, Stonington, CT 06378

⁶Department of Ophthalmology and Visual Sciences, University of Nebraska Medical Center, Omaha, NE 68198

Abstract

Melanopsin, expressed in a subset of retinal ganglion cells, mediates behavioral adaptation to ambient light and other non-image forming photic responses. This has raised the possibility that pharmacological manipulation of melanopsin can modulate several CNS responses including photophobia, sleep, circadian rhythms and neuroendocrine function. Here we describe the identification of a potent synthetic melanopsin antagonist with *in vivo* activity. Novel sulfonamide compounds inhibiting melanopsin (opsinamides) compete with retinal binding to melanopsin and inhibit its function without affecting rod/cone mediated responses. *In vivo* administration of opsinamides to mice specifically and reversibly modified melanopsin-dependent light responses including the pupillary light reflex and light aversion. The discovery of opsinamides raises the prospect of therapeutic control of the melanopsin phototransduction system to regulate light-dependent behavior and remediate pathological conditions.

Users may view, print, copy, download and text and data- mine the content in such documents, for the purposes of academic research, subject always to the full Conditions of use: http://www.nature.com/authors/editorial_policies/license.html#terms

Correspondence, Kenneth A. Jones, kenjones120@gmail.com, Satchidananda Panda, satchin@salk.edu.

*These authors contributed equally to this work.

Authors contribution: KAJ, MH, LSM, JRB, RA, SH, MM, HZ, QZ, and ATEH did the experiments. KAJ, MH, LSM, JRB, ATEH, PJS, GEP, SP and JS analyzed the results and prepared figures. KAJ, JS, ATEH, PJS, GEP and SP designed experiments and prepared the manuscript.

Competing financial interests. Kenneth Jones, Roman Artymyshyn, Sang-Phyo Hong, Mohammad Marzabadi, Huailing Zhong, and Jeffrey Sprouse were employees of Lundbeck Research USA during the period of time that the experimental work was conducted.

Melanopsin (Opn4) and rhodopsin, expressed in the mammalian retina, belong to the opsin family of G-protein coupled receptors (GPCRs) and use *cis* retinal as a chromophore, but they substantially differ in protein sequence, signaling mechanisms, cell type specificity and the light dependent behaviors they control. Melanopsin is expressed in a small subset of retinal ganglion cells that are intrinsically photosensitive (ipRGC) with peak response sensitivity in the blue spectrum¹. Mouse genetics has elucidated key roles of melanopsin in light regulation of the circadian clock, neuroendocrine hormones, pupil diameters, sleep, arousal, photophobia and migraine, while melanopsin is largely dispensable for image-forming function¹. This raises the possibility of pharmacological modulation of melanopsin function to probe its role in non-murine species and a novel therapeutic approach to the treatment of photophobia and light exacerbation of migraine in humans. Migraine pain afflicts nearly 5% of adult males and 15% of females and the cost of treatment and productivity loss in the US alone amounts to >\$17 billion² and references therein). The daily use of tinted glasses that filter out blue light is reported to be effective in attenuating the frequency of childhood migraine³, thus suggesting pharmacological blockade of light input can be an effective therapeutic approach.

Cis retinal binds to opsin photopigments as an inverse agonist and locks them in an inactive conformation. Light-triggered isomerization of *cis* to all-*trans* retinal causes a conformational change in the opsin and activation of a signaling cascade. Photoactivated melanopsin activates Gαq and phospholipase-C that in turn triggers an increase of cytosolic Ca²⁺ from intracellular stores and/or by opening of membrane channels (reviewed in⁴, Supplementary Results, Supplementary Fig. 1a). One of two steps then takes place: melanopsin is thought to photoisomerize the all-*trans* photoproduct to *cis* retinal; alternatively, the all-*trans* retinal is released from melanopsin permitting the apoprotein to bind to new 11-*cis* retinal to regenerate a functional photopigment^{5,6}. Although retinoid derivatives have been extensively used to probe rhodopsin function, their pleiotropic effect on retinoid metabolizing enzymes and nuclear hormone receptors render these compounds as less favorable agents for specific modulation of melanopsin. Here we report a novel screen for small molecule modulators of the melanopsin photoresponse, identification of a non-retinoid class of melanopsin antagonist and demonstration of *in vivo* efficacy of the antagonist in attenuating melanopsin dependent photoresponses in rodents.

Results

Small molecule antagonists of melanopsin

Mammalian rhodopsin and melanopsin share only ~55% amino acid sequence homology within the seven transmembrane region of the protein. Limited sequence similarity is found among the amino acid residues that constitute the retinal binding region of the ground state or light-activated metastate of rhodopsin^{7,8}, suggesting that the interaction of melanopsin with its chromophore is different from that of vertebrate rod/cone opsins. Therefore, we sought to discover antagonists that selectively attenuate the function of melanopsin while sparing that of visual opsins. We adapted a mammalian cell-based assay⁹ to screen for compounds that inhibit melanopsin function. Upon photoexcitation (488 nm, 500 mW), dark-adapted CHO cells stably expressing human melanopsin (CHO^{Opn4}) generated an acute

increase in a Ca^{2+} -dependent fluorescent signal that was absent from host CHO cells lacking ectopically expressed melanopsin (Supplementary Fig. 1b). Pre-exposure of the CHO^{Opn4} cells to white light (1000 lux, 60 min) abolished the photoresponse, which could then be regenerated in a dose-dependent manner with subsequent addition of 9-*cis* retinal, a commercially available analog of 11-*cis* retinal (Supplementary Fig. 2). Immediately after 9-*cis* retinal addition (Supplementary Fig. 2a “Acute addition”), photo-excitation evoked a relatively slow increase in Ca^{2+} that peaked in 25 – 100 s, with a half-maximal effective concentration (EC_{50}) for 9-*cis* retinal of 20 ± 9 nM (Supplementary Fig. 2b). Allowing the light-exposed cells to reconstitute with 9-*cis* retinal for 15 min to 1 h followed by photo-excitation (Supplementary Fig. 2c “Pre-incubation”) led to a rapid Ca^{2+} transient that reached a peak level in <20 s with EC_{50} of 42 ± 18 pM. These results are consistent with the idea that ectopically-expressed melanopsin in CHO cells can be inactivated and likely photobleached by bright light and that the subsequent reconstitution of melanopsin apoprotein with retinal to a fully functional photopigment is a relatively slow process. Such timing might reflect a two-step regeneration process as has been shown for rod/cone opsins¹⁰, in which the retinal is first bound non-covalently to the opsin before the high-affinity Schiff’s base linkage is established. In summary, these results create a framework for carrying out an effective screen for finding antagonists of melanopsin-mediated phototransduction.

We screened 80,000 compounds from the Lundbeck library of diverse compounds (Supplementary Fig. 2 “Screening & Validation”). CHO^{Opn4} cells in 384-well plates were light-exposed, 10 μM of each compound added and following a 30 min incubation period, light-induced increase in Ca^{2+} was measured after addition of 1 μM 9-*cis* retinal. Among the initial hits for compounds that reduced light-dependent Ca^{2+} transients by >2 S.D. from the average response elicited with buffer control, a group of compounds with a common sulfonamide core emerged (Supplementary Table 1). Additional members of the melanopsin-inhibiting sulfonamides (opsinamides) were purchased or synthesized, and tested. Six compounds inhibited melanopsin photoactivation with estimated affinities ranging from 2 – 13,000 nM (Supplementary Table 1 and Supplementary Fig. 3). Two compounds were selected for further characterization based on a combination of affinity and drug-like properties (Fig. 1a and Supplementary Table 3) and a lack of interaction with rhodopsin photopigment isolated from bovine retina (Supplementary Fig. 2d).

While ectopically-expressed melanopsin has been demonstrated to confer photosensitivity to diverse cell types, cell-specific differences in melanopsin’s activation, deactivation, and threshold sensitivity in these various heterologous systems and native ipRGCs have been well documented^{5, 11–14}. In CHO^{Opn4} cells, the opsinamides AA92593 (**1**) and AA41612 (**2**), showed a half-maximal inhibitory concentration (IC_{50}) of 665 ± 9 nM and 15.8 ± 1.8 nM, respectively (Fig. 1a–c). The melanopsin photocurrent from *Xenopus* oocytes ectopically expressing mouse melanopsin⁵ was also inhibited by these two compounds (Fig. 1d and 1e), thus confirming that the inhibition is not restricted to mammalian cells or to specific assay conditions. Pre-incubation of the oocytes with increasing concentrations of AA92593 or AA41612 attenuated melanopsin photocurrent in a dose-dependent manner (Fig. 1d and 1e). Relative potencies of AA92593 (IC_{50} 190 nM) and AA41612 (IC_{50} 20 nM)

in oocytes were comparable to those measured in mammalian cells. The action of AA92593 was found to be highly specific for melanopsin since at a high concentration (10 μ M) it failed to inhibit radioligand binding to a large panel of 74 biological targets including GPCRs and ion channels (Supplementary Table 4).

To elucidate the binding properties of opsinamides for melanopsin, we incubated increasing concentrations of radiolabeled [3 H]₂-AA41612 (Supplementary Fig. 4) with membranes from light-exposed CHO^{Opn4} cells. The amount of bound radioligand in the absence or presence of excess (10 μ M) 9-*cis* retinal was measured to find total, non-specific and specific (total minus non-specific) binding. [3 H]₂-AA41612 exhibited saturable binding to CHO^{Opn4} cell membranes with a maximum binding (B_{max}) of 2.9 pM.mg⁻¹ protein and an equilibrium dissociation constant (K_d) of 0.28 nM (Fig. 2a). The binding isotherm was suggestive of a single binding site within the concentration range tested. Next, we assessed binding reversibility in competition binding experiments. Both agonist (9-*cis* retinal) and unlabeled antagonists (AA41612 and AA92593) exhibited concentration-dependent displacement of [3 H]₂-AA41612 from CHO^{Opn4} cell membranes (Fig. 2b) with Hill slopes close to 1.0 and half-maximal receptor binding concentrations (K_i) of 10.6 \pm 4.0, 0.43 \pm 0.05 and 16 \pm 2 nM, respectively. These results suggest that both the opsinamides and 9-*cis* retinal likely compete for binding to melanopsin. In summary, from the radioligand binding experiments, the opsinamides show saturable and reversible binding to a site that is shared by 9-*cis* retinal.

To functionally assess the nature of inhibition of the melanopsin photoresponse by the opsinamides, we incubated light-exposed CHO^{Opn4} cells with buffer or fixed concentrations of opsinamide, and added increasing doses of 9-*cis* retinal immediately prior to photoexcitation of melanopsin. As expected for a competitive antagonist, increasing doses of opsinamides caused a rightward shift in the retinal dose response curve and consequently a proportional increase in the EC₅₀ for 9-*cis* retinal (Fig. 2c). The dose ratios (DR = EC₅₀ in the presence of antagonist/EC₅₀ in buffer) at different concentrations of opsinamide were used to create Schild plots (Fig. 2d). Although maximal efficacy was slightly reduced at high concentrations of antagonist, the slope of the Schild plot was not significantly different from 1.0, which further suggested that opsinamides and 9-*cis* retinal compete for their actions on melanopsin.

Estimation of compound affinities to previously light-exposed melanopsin using the Schild plot determined the apparent K_b values of 160 \pm 55 nM and 6.2 \pm 1.1 nM for AA92593 and AA41612, respectively. However, in the retina, melanopsin-based responses can be further enhanced by addition of exogenous retinal^{15, 16}, thus suggesting that a mixture of retinal-free apoprotein and retinal bound melanopsin exist in the ipRGCs. To test the potency of the antagonist in inhibiting melanopsin-*cis*-retinal photopigment, light-exposed CHO^{Opn4} cells were first incubated for 15 min with a range of 9-*cis* retinal concentrations to form functional photopigment before the antagonist was added. Subsequent measurement of the melanopsin photoresponse revealed diminished antagonist potency. For example, the apparent K_b of AA92593 was reduced from 160 nM to approximately 6 μ M. This is consistent with the higher affinity of *cis*-retinal for melanopsin (EC₅₀ 42 pM; Supplementary Fig. 2), and slow off-rate of *cis*-retinal from Schiff's base linkage with the

opsin. Taken together, these results suggest that low μM concentrations of AA92593 should be capable of inhibiting photoactivation of ipRGCs *in situ*.

Opsinamide inhibits native ipRGC photoresponses

To test whether opsinamides can inhibit melanopsin-dependent photoresponses in native ipRGCs, immunopanned rat ipRGCs were repeatedly stimulated with 1 min light pulses with a 15 min inter-pulse interval and the light-evoked rise in intracellular Ca^{2+} levels was measured using the ratiometric calcium indicator dye Fura-2¹⁴. In solvent treated cells (n=14) response magnitude to the 1 min light pulse slightly increased during the recording period (i.e. 8 light pulses over 110 min – Fig. 3a). Application of 10 μM AA92593 to ipRGCs showing normal light responses to 2 test pulses reduced the photoresponse to successive light pulses such that the responses to the last two light pulses were suppressed by more than 90% compared to the solvent-treated cells (Fig. 3b). Since the light-induced increase in intracellular Ca^{2+} is largely the result of Ca^{2+} influx through voltage-dependent calcium channels activated after action potential firing¹⁴, the data suggest that AA92593 inhibits isolated ipRGCs from firing action potentials in response to light, and hence might also attenuate melanopsin-mediated light responses in the intact retina.

In anticipation of *in vivo* studies, we performed a pharmacokinetic analysis of AA92593 and associated opsinamides. Systemic dosing with AA92593 yielded measurable exposure in both brain and retina. Following 30 mg kg^{-1} IP, tissue levels remained high ($>2,000$ ng. g^{-1} tissue weight or ~ 7.5 μM) in the retina 30 min after administration, and subsequently $>95\%$ was rapidly cleared within 2 h (Fig. 3c), thus offering a sufficient temporal window to monitor *in vivo* efficacy and reversibility. Given its apparent K_b of 160 nM in CHO^{Opn4} cells pre-exposed to light and ~ 6 μM in cells reconstituted with retinal, this dose of AA92593 should deliver enough antagonist in the retina to inhibit both the apoprotein as well as a fraction of the retinal-bound melanopsin leading to significant attenuation of the melanopsin mediated photoresponses.

For *in vivo* studies, we first tested the effect of AA92593 on different photoreceptor classes in intact retina. Both wild type (WT) C57BL/6J mice (Supplementary Fig. 5) and melanopsin-deficient mice (*Opn4*^{-/-}) (Fig. 3d and 3e) with intact rod/cone functions treated with AA92593 showed no noticeable inhibition of rod/cone photoreceptors as their rod- and rod/cone combined electroretinograms (ERGs), recorded within 30 min of compound administration, were similar to those of vehicle-treated control mice. Furthermore, opsinamide did not significantly attenuate dark recovery of rod responses after a saturating light pulse, thus suggesting opsinamides do not adversely affect rod photopigment function (Fig. 3f and g and Supplementary Fig. 6).

To test whether opsinamide inhibits light-evoked ipRGC action potential firing, we recorded light responses from retinas from C3H/HeJ (*rd*) mice. These animals carry the *Pde6b* mutation that causes progressive loss of most of their rod and cone photoreceptors soon after birth and the adult mice (> 3 months old) largely express only melanopsin photopigment in the retina¹⁷. As direct perfusion of drugs known to inhibit melanopsin downstream signaling steps is relatively ineffective in accessing ipRGCs in intact retina preparations¹⁸, we adapted a method that leverages the natural drug delivery through the retinal

microvasculature. We injected adult *rd* mice with AA92593 or vehicle prior to harvesting retinas. ipRGC action potential firing in response to a 1 min light pulse in retinas pre-treated with AA92593 was reduced by >70% compared to controls. Upon washout of the opsinamide, light induced spike number gradually returned within 30 min to the response pattern observed in the retina from mice pre-treated with vehicle alone (Fig. 3h–j and Supplementary Fig. 7).

Opsinamide inhibits melanopsin dependent behaviors

Next, we assessed the effect of AA92593 on the pupillary light reflex (PLR) in adult *rd* mice. As ipRGCs are in essence the only functional photoreceptor type present in these mice, they offer a large dynamic range for evaluating melanopsin sensitivity in intact animals via the PLR^{17,19}. AA92593 dosed i.p. (30 mg kg⁻¹) 20 min prior to PLR measurement attenuated pupil constriction in response to light (10¹³ ph.cm⁻².s⁻¹) by ~50% (Fig. 4a and b and Supplementary Fig. 8). Up to 30 min after opsinamide treatment, the mice exhibited slow constriction, reduced maximum constriction and faster relaxation. Such PLR perturbation was reversible; resumption of normal PLR response within 60 min paralleled opsinamide clearance from the retina (Fig. 3c). This close correlation between duration of drug availability in the retina (Fig. 3c) and inhibition of the PLR also suggests that the opsinamides do not cause irreversible or long lasting changes in the signaling circuitry from melanopsin activation to pupil constriction. In mice with intact rod/cone photoreceptors, melanopsin contributes to PLR at high irradiance (>10¹² ph.cm⁻².s⁻¹) and there is sufficient separation of pupil constriction between rod/cone (*Opn4*^{-/-} mice) and rod/cone+melanopsin (WT mice) photoreceptor systems (see Fig. 2b from²⁰) to detect any drug effect. Wild type (WT) mice treated with AA92593 showed attenuated PLR under high light intensity (10¹³ ph.cm⁻².s⁻¹). PLR in *Opn4*^{-/-} mice, PLR at low light intensity (10¹⁰ ph.cm⁻².s⁻¹) in WT mice, and the initial (up to 1 s) pupil constriction speed in both WT and *Opn4*^{-/-} mice are driven by rod/cone photoreceptors^{20,21} and are unaffected by opsinamide (Fig. 4c–e, Supplementary Fig. 8e), thus demonstrating no appreciable off-target effect of the antagonist on this phenotype. Constriction speed after the first 1s at high irradiance is dependent on melanopsin and are attenuated by opsinamide. Altogether these results support the conclusion that AA92593 functions as a specific inhibitor of melanopsin and has no detectable adverse effect on rod/cone-mediated light responses *in vivo*.

The ipRGCs send their axons to several thalamic regions including the ventral lateral posterior thalamic nuclei and dorsal posterior thalamic nuclear group where they have been shown to make synaptic contacts with dura-sensitive neurons²². This forms the neural basis for light exacerbation of migraine pain or photophobia impairing learning in young children and productivity in adults. Wearing orange tinted glasses for a few hours daily that filter out melanopsin-activating blue light reduces migraine attacks³. A specific contribution of melanopsin to light aversion in rodents is clearly evident in young rodent pups²³. Neonatal mice (<P14) have fully functional ipRGCs prior to the establishment of a functional rod/cone photoreceptor system. By this age, the ipRGC axons already innervate their major brain targets (Supplementary Fig. 9). WT pups showed strong aversion to blue light that matches the peak spectral sensitivity of melanopsin (Fig. 4f–h, Supplementary Fig. 10 and Supplementary Movie 1). These pups showed exploratory activity under darkness. Light

stimulus triggers an avoidance response in which they turn their head, move away from the light source and then stop activity. *Opn4*^{-/-} mice lack such aversion behavior to blue light (Supplementary Movie S2). WT pups injected with AA92593 exhibit remarkably reduced light aversion behavior and phenocopied *Opn4*^{-/-} pups (Supplementary Movie 3); light did not acutely trigger a negative phototaxis and the pups continued to be active for a prolonged period of time after the onset of a light stimulus.

Discussion

In summary, we report a non-retinoid, first-in-class, highly specific compound targeting the photopigment melanopsin that effectively and reversibly suppresses non-visual photoresponses in the intact mouse without affecting overall rod/cone photoreceptor function. The selectivity most likely arises from the primary amino acid sequence divergence between melanopsin and rod/cone opsins. Vertebrate rod/cone opsins and melanopsin share only limited primary amino acid sequence similarity^{24, 25} and employ distinct retinal use and signaling properties^{5, 11, 12, 26}. Sequence comparison of mouse or human melanopsin with published crystal structures of bovine rhodopsin reveals that nearly half of the key residues that directly support retinal dynamics in ground state or photoactivated state^{7, 8, 27, 28} are not conserved. They include T94F, E113Y, A117G, T118A, E122I, W126I, C185T, I189W, Y192M, A269S, F273L, F293V (single letter amino acid code and position in bovine rhodopsin followed by the aminoacid in the respective position in mouse melanopsin are indicated).

The potency of opsinamide likely depends on the retinal-bound state of melanopsin. Its binding to melanopsin apoprotein is competitive, thereby interfering with subsequent binding of retinal. There are at least two different explanations for the observed attenuation of melanopsin mediated photoresponses by opsinamide *in vivo* without prior light exposure of the mouse retina. First, there is evidence that sufficient melanopsin apoprotein exists in the retina^{15, 16}, which may be blocked by opsinamide from reconstitution with retinal. We currently do not know whether, as proposed for rhodopsin²⁹, melanopsin also exists as a dimer and whether both dimeric partners are required to have bound retinal for normal function. So, in this scheme opsinamide bound melanopsin can render the dimeric complex inactive even if its partner molecule harbors bound retinal. Second, opsinamide at a higher concentration (~6 μ M) can inhibit melanopsin reconstituted with retinal. The amount of opsinamide retained in the retina up to 30 min after administration is in this range, and hence can inhibit melanopsin by displacing retinal. The extent of PLR attenuation using doses of opsinamide consistent with *in vitro* models and the lack of off-target effects as seen from *Opn4*^{-/-} mice, support the conclusion that opsinamides inhibit melanopsin function and sufficient quantity of opsinamide reaches the retina so that it does not require substantial prior photoactivation to achieve melanopsin inhibition.

Although opsinamides exhibit nanomolar potency against melanopsin apoprotein, the higher affinity of *cis*-retinal for melanopsin (EC₅₀ 42 pM; Supplementary Fig. 2), and the slow off-rate of *cis*-retinal from the Schiff's base linkage with the opsin, may explain the incomplete inhibition of melanopsin response *in vivo*. Nevertheless, the magnitude of inhibition is large enough to ameliorate light aversion and produce significant inhibition of melanopsin-

mediated PLR in adult mice. The results indicate that targeting melanopsin is a novel and tractable therapeutic option for treating light-modulated disorders of the central nervous system, such as migraine and photophobia. Current therapies for these disorders are either non-existent, or in the case of migrain they leave residual symptoms such as photophobia. The discovery of these compounds against the opsin class of receptors now opens up the possibility that a similar strategy can be taken to identify new pharmacological modulators of other opsins including classical rhodopsin to treat vision problems related to excessive activation of rhodopsin. Furthermore, these compounds also offer a novel pharmacological tool to evaluate the function of melanopsin in non-model organisms that are not easily amenable to genetic perturbations.

Online Methods

Ethics statement

All animal studies were approved by Institutional Animal Care and Use Committee of the Salk Institute for Biological Studies, and University of Nebraska, and performed in accordance with the guidelines.

Cloning and expression of melanopsin (Opn4)

Human, mouse, and rat melanopsin cDNA was cloned using standard methods. Cloned sequences correspond to the following sequences currently available: human NM_033282.31, Rat NM_138860.1, and mouse NM_013887.2. Stable cell lines were generated by co-transfection of plasmid DNA encoding melanopsin with a second plasmid conferring neomycin resistance into CHO cells. Clones were selected using the Ca^{2+} release assay (below). Cells were maintained in DMEM media with 10% FCS in the presence of neomycin.

Ca^{2+} release assays

CHO cells stably expressing human melanopsin (CHO^{Opn4}) were treated with trypsin and seeded onto poly D-lysine coated Costar 384-well plates (12,000 cells/well) and incubated overnight in serum-free medium. For most experiments, 2 h prior to assay, the cells were exposed to ~1,000 lux light from a white fluorescent light source at room temperature for 1 h. Cell medium was removed, and cells were washed once with 70 μl of assay buffer (Hank's Balanced Salt solution supplemented with 20 mM HEPES, 2.5 mM probenecid and 0.05% BSA). Cells were loaded with calcium indicator Fluo-4 AM (Molecular Probes) using a MultiDrop fluid dispenser, and incubated for 1 h at 37° C in a CO_2 incubator, and then washed three times with assay buffer. For high-throughput screening, compounds (10 μM final concentration) were first added to cell plates and incubated for 30 min. Cell plates were placed in FLIPR384 (MDS Molecular Devices), and fluorescence was measured every 1 s for up to 30 s before addition of 1 μM 9-*cis* retinal. Fluorescence measurement was continued for up to 2 min after retinal addition. Because the assay was done in non-equilibrium condition, it was more reliable to measure antagonist potencies by calculating compound K_b ³⁰. This was performed by measuring 9-*cis* retinal EC_{50} s in the absence and presence of antagonist (1 or 10 μM). The magnitude of the parallel curve shift is a function of antagonist potency in a competitive system. K_b values were calculated using the equation:

$\log K_b = \log[B] - \log(DR-1)$, where B is the concentration of antagonist used and DR is the ratio of the EC_{50} s in the absence and in the presence of antagonist.

Concentration-effect data were fitted to sigmoidal curves using Prism software (GraphPad Software). Schild plots showing the effects of increasing concentrations of antagonist on 9-*cis* retinal concentration-effect curves were prepared as described³¹. In some experiments, the 9-*cis* retinal was added after dye loading and 15 min later the compounds were added.

Sulfonamides

Opsinamides AA92593 and AA41612 were from Princeton Biomolecular Research (>98% purity), AE51310, AA73920 and AD83947 from ChemBridge (>90% purity), and AD96765 from Interchim (>90% purity). 1-((2,5-dichloro-4-methoxyphenyl)sulfonyl)piperidine-3,4-t₂ (Radio ligand [³H]₂-AA41612) was prepared as follows. The reaction of 2,5-dichloro-4-methoxybenzene sulfonyl chloride (compound **7** in Supplementary Fig. 4, Ryan Scientific, Purity>90%) with the commercially available 1,2,3,6-tetrahydropyridine, followed by hydrogenation using 10% Pd/C in ethyl acetate was duplicated using tritium (T₂) at ARC (American Radiolabeled Chemicals, Inc.) to yield 1-((2,5-dichloro-4-methoxyphenyl)sulfonyl)piperidine-3,4-t₂ (compound **8**): The purity of compound **8** was determined by HPLC to be 98% (Zorbax C-18; 1% TFA in H₂O / acetonitrile (10%–100%); detection: UV at 254 nm and ³H β-Ram); Specific activity of compound **8** = 50 Ci/mmol.

Radioligand binding assays

Cell membranes from CHO^{Opn4} cells were prepared by harvesting whole cells and disrupting the cell pellet by sonication in ice-cold buffer (20 mM Tris-HCl, 10 mM EDTA, pH 7.4 at 4 °C). The resulting crude cell lysate was cleared of cell debris by low speed centrifugation at 200g for 5 min at 4°C. The cleared supernatant was then centrifuged at 40,000g for 20 min at 4°C, and the resulting membrane pellet was washed by suspending in ice-cold buffer and repeating the high speed centrifugation step. The final washed membrane pellet was re-suspended in assay buffer containing: 50 mM Tris-HCl, 1 mM EDTA, 5 mM MgSO₄, pH 7.4. Protein concentration was determined by the Bradford method.

In equilibrium saturation binding assays, isolated membranes were incubated in assay buffer with increasing concentrations of [³H]₂- AA41612. In equilibrium competition binding assays, isolated membranes were incubated with 300 pM of the radioligand in the presence of increasing concentrations of competing ligand for 2 h in the dark at 25 °C. Binding reactions were stopped by filtration through a double layer of glass fiber filters treated with 0.1% polyethyleneimine using a cell harvester. Radioactivity was measured by scintillation counting (Trilux). Nonspecific binding was defined as the amount of radioactivity remaining in the presence of 10 μM 9-*cis* retinal.

Melanopsin photoactivation in *Xenopus* oocytes

In vitro transcribed and polyadenylated mRNAs for mouse melanopsin, TrpC3, Gαq and Arrb1 were injected into stage IV *Xenopus* oocytes, and intracellular recording of melanopsin photocurrent was carried out as described earlier⁵. Opsinamide AA92593 was diluted to desired concentration and perfused for 3 min prior to addition of 50 μM 11-*cis*

retinal. Subsequent light stimulation and intracellular recordings were carried out as described earlier⁵.

Isolated rat ipRGC photoactivation

Long Evans rats were sacrificed at 5–6 days postnatal, and the retinas were dissected and dissociated into a single cell suspension. Purified cultures of ipRGCs were generated using a two-step immunopanning technique involving rabbit anti-rat N-terminus melanopsin antibodies as in previous work (12). The cells were plated onto coverslips in serum-free Neurobasal A+B27 medium with BDNF, CNTF, forskolin and gentamicin and calcium imaging was performed on the cells after 1 to 3 days in culture. The ipRGCs were loaded with the calcium indicator dye Fura-2 AM for 30 min under dark conditions before being placed into the recording chamber positioned on an upright fluorescence microscope (Zeiss Axioskop 2 FS). Cells were continuously perfused with oxygenated Hanks buffer medium warmed to 33 – 35°C using an inline heater. Once cells were visually located under the 40X water-immersion objective, a test light pulse was given to ensure cells in the field of view responded with an increase in intracellular Ca^{2+} levels (recorded as a change in ratio of emitted fluorescence at 510 nm after excitation at 340 nm and 380 nm). Each light pulse (broad-spectrum light from a 100 W halogen bulb, with same irradiance as used in previous work [12]) was 1 min in duration and images were captured every 10 s during the light pulse and every minute between pulses while the cells were maintained in complete darkness. The initial two light pulses were used to create a baseline response, and subsequent light pulses were given every 15 min. Perfusion of the melanopsin antagonist (10 μ M) into the chamber followed the 2nd light pulse, and the antagonist was then perfused continuously for the remainder of the recording session; experiments typically consisted of 8 light pulses after which time the calcium indicator was no longer effective.

Bioanalysis for pharmacokinetics

Frozen brains were weighed and homogenized in four volumes (w/v) of homogenization buffer consisting of 50% water, 30% 2-propanol and 20% DMSO. A 150 μ l internal standard solution (AA92593 in 80% acetonitrile/ 20% DMSO) was added to 50 μ l homogenized brain/plasma sample. The samples were mixed and centrifuged. The supernatant was injected directly into a ThermoFinnigan Quantum Ultra LC/MS/MS system for analysis. A standard curve (0 – 5,000 ng/ml) was generated in homogenates to determine the concentrations of AA92593 in the brain.

Electroretinogram (ERG)

WT or *Opn4*^{-/-} mice were dark adapted for 2 h before testing, and all ERGs were recorded under dim red light illumination. First, mice were anesthetized with a mixture of Ketamine (100 mg/kg) and Xylazine (10 mg/kg). Their pupils were dilated with a drop of tropicamide, and wire electrodes were positioned on each eye. Reference electrode and ground were placed respectively on the forehead and the leg of the animal. Measurements were done as described earlier³² or with the Espion E² Visual Electrophysiology System (Diagnosys, LLC) which controls acquisition, amplification, filtering (0.312 to 100 Hz), stimulation and timing. The signal is digitized at 1 kHz. The stimuli consisted of brief full field flashes

(pulses color: white 6500K). Each response corresponded to the averaging of 4 trials spaced by 10 s. We recorded from 50 ms before the flash to 200 ms after.

The program saved the data to a text file, which was imported into an analysis program written in Matlab. The a-wave amplitude was measured from the baseline to the trough of the a-wave, and b-wave amplitude was measured from the trough of the a-wave to the top of the b-wave. The a-wave implicit time was measured from the beginning of the stimulus to the trough of the a-wave, and the b-wave implicit time was measured from the beginning of the stimulus to the top of the b-wave.

Multi Electrodes Array (MEA) recording

Initial experiments, using rd mice and neonatal rat retinas, indicated that the bath application of the opsinamide required high concentrations (~100 μM) of this compound for significant effects on ipRGC light responses to be observed. This is likely due to the poor drug diffusion in this preparation (intact retina placed RGC-side down on the MEA), in which the drug has to perfuse through the outer retina to the fine ipRGC dendrites embedded deep in the tissue (see [16] for discussion of diffusion issues). In view of this physical limitation, the opsinamide was instead delivered systemically through IP injections performed prior to the MEA recordings. Dark-adapted adult rd mice received either AA92593 (30 mg kg^{-1}) or vehicle via IP injection 15 min prior to sacrifice. After removal from the eye, a patch of retina about 4 – 10 mm^2 was mounted on a Multi-electrode array (Multichannel Systems, Reutlingen, Germany), ganglion cell side down, and perfused with oxygenated Ames' medium at 35 °C supplemented with 20 μM CNQX and 50 μM D-APV to block glutamatergic transmission. Retinas were dissected and incubated in medium containing 10 μM AA92593 or vehicle until the first light pulse, after which recordings were conducted in medium containing vehicle only (washout). The activity of ganglion cells was recorded via 256 electrodes 30 μm in diameter spaced every 100 μm apart and arranged in a 16 \times 16 square grid. Full-field visual stimuli at a flux of 5×10^{12} photons/ cm^2/s at the retina was presented during recordings using a high brightness LED (LuxeonStar 5, luxeonstar.com) with a peak wavelength of 480 nm. The current through the LED was controlled using custom electronics and software written in Matlab (Mathworks, Natick, MA) and aligned with the physiological recording with a resolution of ± 100 μs . Signal was acquired from all 256 channels at 10 kHz. Negative thresholds for spike detection were set at 5 times the standard deviation of the noise on each channel. Spike cutouts, consisting of 1 ms preceding and 2 ms after a suprathreshold event, along with a time stamp of the trigger were collected. For each electrode, these spike cutouts were sorted into trains of a single cell using Offline Sorter (Plexon, Denton, TX). Data analysis and display were performed using Neuroexplorer (Plexon) and custom software written in Matlab.

Response threshold was fixed at the baseline discharge rate (average of the rate measured over the 30 s preceding light ON) plus two times the standard deviation. A cell was considered to respond from the time its firing rate went above the threshold (for at least 2 s) to the time it returned to threshold (for at least 2 s). Duration of the response and the number of spikes fired in this interval were analyzed.

Pupillary light reflex (PLR)

Mice were implanted with an acrylic headpost. After at least 1 wk of recovery from the headposting surgery, they were tested for PLR. On the day of the testing, 20 min before the first light stimulation, dark-adapted mice received an IP injection of either vehicle or compound (30 mg kg⁻¹ body weight of mouse) as well as a drop of tropicamide in the left eye. Before the recordings, mice were briefly anesthetized with isoflurane and restrained in a custom-made animal holder. The animal holder was placed inside a light tight box with the left eye apposed against an opening of an integrating sphere. Light from a 300 Watt Xenon Arc lamp light source (Sutter Instrument, Novato, CA, USA) was filtered, collimated and delivered to the integrating sphere through a liquid light guide. An inline 480 nm filter, a filter wheel with a neutral density filter and a Lambda 10–3 optical filter changer with SmartShutter™ were used to control the spectral quality, intensity and duration of light. Light intensity was measured with a Melles Griot power meter. The mouse's right eye was illuminated by an IR LED and recorded with a high precision LINX video camera (Imperx Inc.) equipped with an IR filter at a sample rate of 30Hz. We recorded 5 min sequences consisting of 1 min of darkness, 1 min of monochromatic 480 nm light (1×10^{13} ph.cm⁻².s⁻¹ or 1×10^{10} ph.cm⁻².s⁻¹) and finally 3 min of darkness. This sequence was repeated 19 min, 29 min and 39 min after the injection. Digital movies of pupil constriction were analyzed with a custom Labview (National Instruments) program. We extracted the pupil diameter. The mean diameter measured during the first period of darkness (20 s) of each sequence served as the baseline for normalization of the recordings. Note the bright light used is known to isolate the specific contribution of melanopsin to PLR in multiple studies including the irradiance response curve shown in Lucas et al. However, the intensity used here is not the brightest intensity used in Lucas et al ($7E14$ ph.cm⁻².s⁻¹; see [18]).

Negative phototaxis assay

WT and *Opn4*^{-/-} pups aged from P7 to P9 were tested in a phototaxis assay (once a day) with the procedure modified from 21. After the mouse pups were dark adapted for 1 h, they received a sub-cutaneous injection of either vehicle or AA92593 (30 mg kg⁻¹ body weight of mouse). A small (3 mm diameter) reflective dome sticker was placed on their head for video tracking and the pup was placed inside a transparent cylindrical plexiglass tube for 10 min. After the first 5 min under total darkness, the end of the tube where the mouse head was pointed at was illuminated with bright monochromatic 480 nm light (9.5×10^{15} ph/cm²/s measured closet to the light). The tube was illuminated with 2 infrared (IR) LED bars (Environmental Light™) and the pup's activity was video recorded during the last 7 min (2 min before and 5 min after light ON) with a Sony video camera equipped with an IR filter. Digital movies were then analyzed offline with a custom centroid detection-based program implemented in Matlab (Mathworks). We extracted the distance covered by the head in 1 s bins that allowed us to obtain the pups activity profile during the recording as well as to compare the mean activity before and after light on. Pups that didn't show significant activity (no bin with above 1.3 mm/bin or 5 pixels/bin threshold) during the 2 min before light ON were excluded from the analysis. Cnetral projections of melanopsin RGCs in P8 pups were stained in *Opn4*^{Cre/+};Z/AP mouse³³.

Supplementary Material

Refer to Web version on PubMed Central for supplementary material.

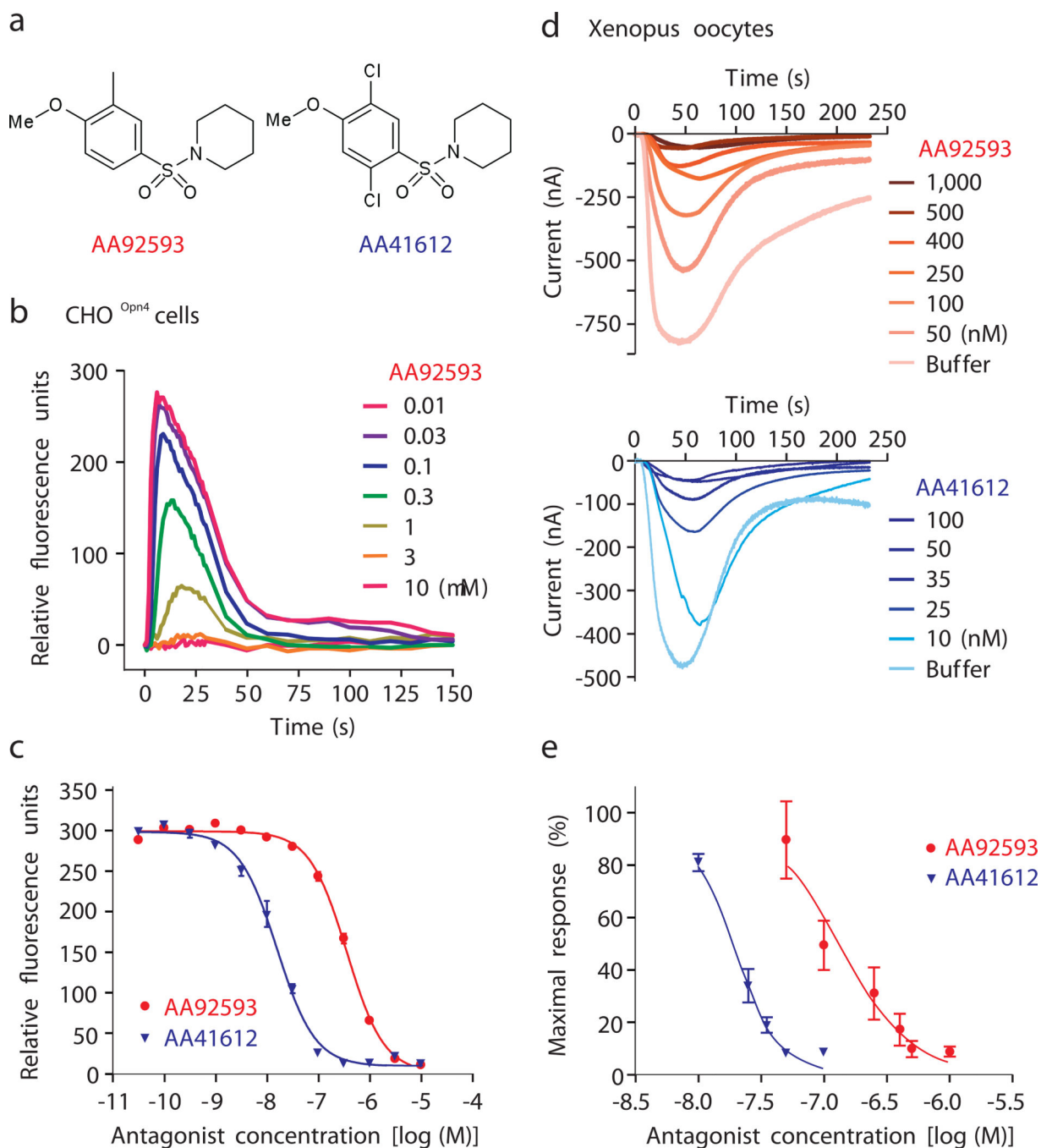
Acknowledgments

We thank Noel Boyle, Boshan Li, Asanthi Pieris, Rui Li, Priya Rao, Manual Cajina, Hong Zhang (Lundbeck), Hiep Le, Sheena Keding (Salk Institute) for expert technical help. This work was supported by grants from the Hearst Foundation, NIH EY 016807, S10 RR027450, and NS066457 to S.P., JSPS fellowship to M.H., Fyssen and Catharina foundation fellowships to L.S.M., NIH EY017809 to P.J.S. and G.E.P.

References

1. Hatori M, Panda S. The emerging roles of melanopsin in behavioral adaptation to light. *Trends Mol Med*. 2010
2. Pryse-Phillips WE, et al. Guidelines for the diagnosis and management of migraine in clinical practice. *Canadian Headache Society. CMAJ : Canadian Medical Association journal = journal de l'Association medicale canadienne*. 1997; 156:1273–1287.
3. Good PA, Taylor RH, Mortimer MJ. The use of tinted glasses in childhood migraine. *Headache*. 1991; 31:533–536. [PubMed: 1960058]
4. Do MT, Yau KW. Intrinsically photosensitive retinal ganglion cells. *Physiol Rev*. 2010; 90:1547–1581. [PubMed: 20959623]
5. Panda S, et al. Illumination of the melanopsin signaling pathway. *Science*. 2005; 307:600–604. [PubMed: 15681390]
6. Walker MT, Brown RL, Cronin TW, Robinson PR. Photochemistry of retinal chromophore in mouse melanopsin. *Proc Natl Acad Sci U S A*. 2008; 105:8861–8865. [PubMed: 18579788]
7. Choe HW, et al. Crystal structure of metarhodopsin II. *Nature*. 2011; 471:651–655. [PubMed: 21389988]
8. Okada T, et al. The retinal conformation and its environment in rhodopsin in light of a new 2.2 Å crystal structure. *J Mol Biol*. 2004; 342:571–583. [PubMed: 15327956]
9. Pulivarthy SR, et al. Reciprocity between phase shifts and amplitude changes in the mammalian circadian clock. *Proc Natl Acad Sci U S A*. 2007; 104:20356–20361. [PubMed: 18077393]
10. Kefalov VJ, Crouch RK, Cornwall MC. Role of noncovalent binding of 11-cis-retinal to opsin in dark adaptation of rod and cone photoreceptors. *Neuron*. 2001; 29:749–755. [PubMed: 11301033]
11. Melyan Z, Tarttelin EE, Bellingham J, Lucas RJ, Hankins MW. Addition of human melanopsin renders mammalian cells photoresponsive. *Nature*. 2005; 433:741–745. [PubMed: 15674244]
12. Qiu X, et al. Induction of photosensitivity by heterologous expression of melanopsin. *Nature*. 2005; 433:745–749. [PubMed: 15674243]
13. Wong KY, Dunn FA, Berson DM. Photoreceptor adaptation in intrinsically photosensitive retinal ganglion cells. *Neuron*. 2005; 48:1001–1010. [PubMed: 16364903]
14. Hartwick AT, et al. Light-evoked calcium responses of isolated melanopsin-expressing retinal ganglion cells. *J Neurosci*. 2007; 27:13468–13480. [PubMed: 18057205]
15. Fu Y, et al. Intrinsically photosensitive retinal ganglion cells detect light with a vitamin A-based photopigment, melanopsin. *Proc Natl Acad Sci U S A*. 2005; 102:10339–10344. [PubMed: 16014418]
16. Do MT, et al. Photon capture and signalling by melanopsin retinal ganglion cells. *Nature*. 2009; 457:281–287. [PubMed: 19118382]
17. Panda S, et al. Melanopsin is required for non-image-forming photic responses in blind mice. *Science*. 2003; 301:525–527. [PubMed: 12829787]
18. Berson DM. Phototransduction in ganglion-cell photoreceptors. *Pflugers Arch*. 2007; 454:849–855. [PubMed: 17351786]
19. Lucas RJ, Douglas RH, Foster RG. Characterization of an ocular photopigment capable of driving pupillary constriction in mice. *Nat Neurosci*. 2001; 4:621–626. [PubMed: 11369943]

20. Lucas RJ, et al. Diminished pupillary light reflex at high irradiances in melanopsin-knockout mice. *Science*. 2003; 299:245–247. [PubMed: 12522249]
21. Lall GS, et al. Distinct contributions of rod, cone, and melanopsin photoreceptors to encoding irradiance. *Neuron*. 2010; 66:417–428. [PubMed: 20471354]
22. Nosedá R, et al. A neural mechanism for exacerbation of headache by light. *Nat Neurosci*. 2010; 13:239–245. [PubMed: 20062053]
23. Johnson J, et al. Melanopsin-dependent light avoidance in neonatal mice. *Proc Natl Acad Sci U S A*. 2010; 107:17374–17378. [PubMed: 20855606]
24. Provencio I, Jiang G, De Grip WJ, Hayes WP, Rollag MD. Melanopsin: An opsin in melanophores, brain, and eye. *Proc Natl Acad Sci U S A*. 1998; 95:340–345. [PubMed: 9419377]
25. Nayak SK, Jegla T, Panda S. Role of a novel photopigment, melanopsin, in behavioral adaptation to light. *Cell Mol Life Sci*. 2006; 64:144–154. [PubMed: 17160354]
26. Isoldi MC, Rollag MD, Castrucci AM, Provencio I. Rhabdomeric phototransduction initiated by the vertebrate photopigment melanopsin. *Proc Natl Acad Sci U S A*. 2005; 102:1217–1221. [PubMed: 15653769]
27. Palczewski K, et al. Crystal structure of rhodopsin: A G protein-coupled receptor. *Science*. 2000; 289:739–745. [PubMed: 10926528]
28. Standfuss J, et al. The structural basis of agonist-induced activation in constitutively active rhodopsin. *Nature*. 2011; 471:656–660. [PubMed: 21389983]
29. Jastrzebska B, Orban T, Golczak M, Engel A, Palczewski K. Asymmetry of the rhodopsin dimer in complex with transducin. *FASEB J*. 2013; 27:1572–1584. [PubMed: 23303210]
30. Craig DA. The Cheng-Prusoff relationship: something lost in the translation. *Trends Pharmacol Sci*. 1993; 14:89–91. [PubMed: 8488569]
31. Kenakin, TP. *A Pharmacology Primer: Theory, Application and Methods*. London: Elsevier Academic Press; 2006.
32. Hatori M, et al. Inducible ablation of melanopsin-expressing retinal ganglion cells reveals their central role in non-image forming visual responses. *PLoS ONE*. 2008; 3:e2451. [PubMed: 18545654]
33. Brown TM, et al. Melanopsin contributions to irradiance coding in the thalamo-cortical visual system. *PLoS Biol*. 2010; 8:e1000558. [PubMed: 21151887]

**Fig. 1.**

Opsinamides inhibit melanopsin photoresponse. (a) High-throughput screen of a small molecule library and subsequent medicinal chemistry identified two sulfonamides with sufficient potency against melanopsin. AA92593 [1-(2,5-Dichloro-4-methoxybenzenesulfonyl)-piperidine] and AA41612 [1-(4-Methoxy-3-methyl-benzenesulfonyl)-piperidine]. (b) Increasing concentrations of AA92593 correspondingly reduced the light-induced rise in cytosolic Ca²⁺ in CHO^{Opn4} cells. Real-time cellular Ca²⁺ changes after the addition of AA92593 was measured with Fluo-4 based dye. (c) Dose-dependent reduction in

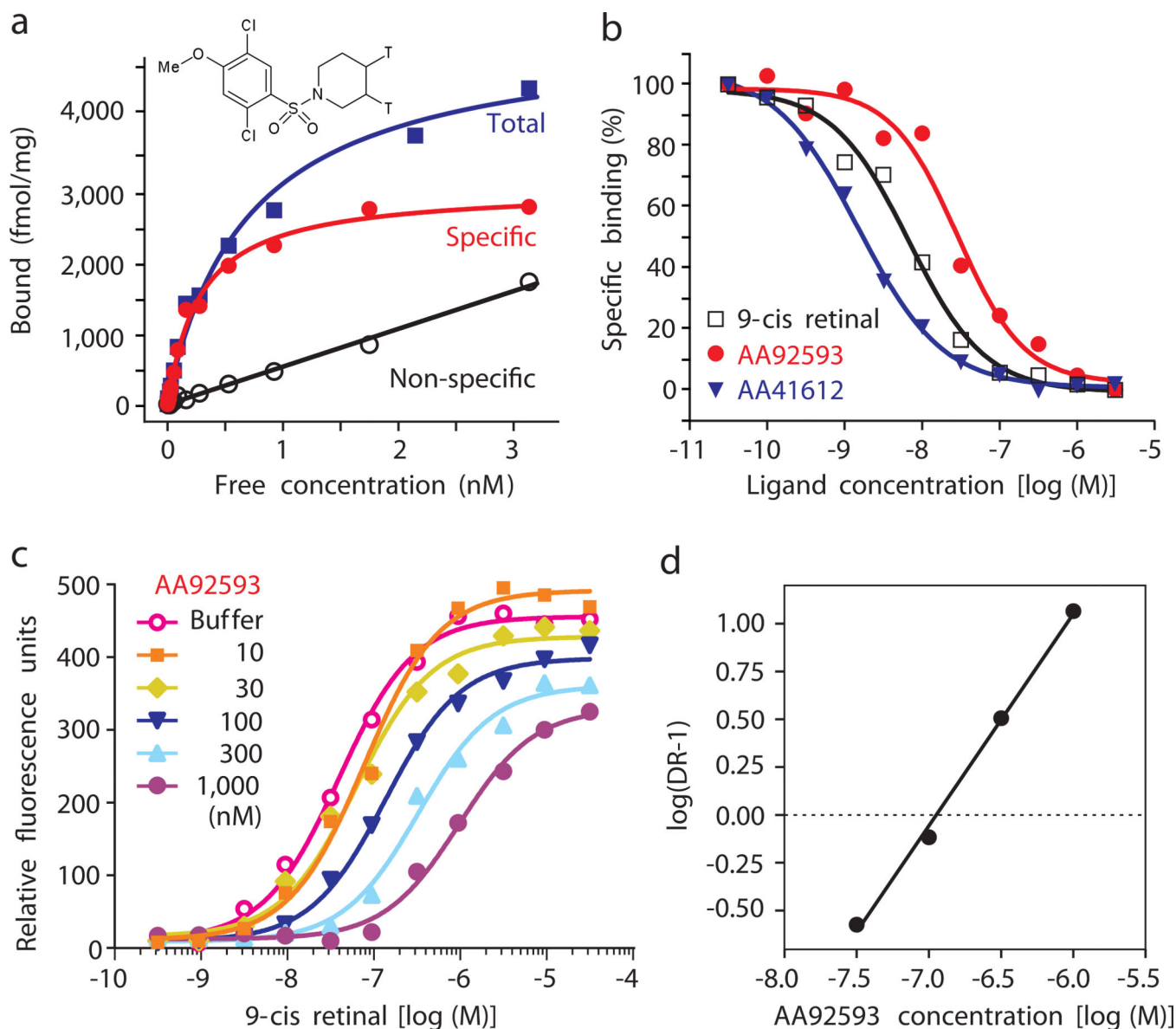
peak light-induced Ca^{2+} fluorescence from CHO^{Opn4} cells pre-incubated with increasing concentration of AA92593 or AA41612. Average response (\pm S.E.M., $n = 4$ wells) plotted against different concentrations of antagonist or buffer control illustrates higher potency of AA41612. **(d)** Both opsinamides also inhibited light-induced melanopsin photocurrent in *Xenopus* oocytes. Average response ($n = 5$ oocytes) to 60 s of white light are shown. **(e)** Normalized average photocurrent (\pm SEM, $n = 5$) plotted against increasing concentrations of opsinamides showed AA41612, as seen in mammalian cells, is more potent inhibiting melanopsin than AA92593.

Author Manuscript

Author Manuscript

Author Manuscript

Author Manuscript

**Fig. 2.**

Specific and competitive binding of opsinamide to melanopsin. **(a)** Specific binding of [^3H] $_2$ - AA41612 to melanopsin and displacement by unlabeled AA41612. Radiolabeled [^3H] $_2$ - AA41612 showed saturable binding to membrane fraction from light-exposed CHO^{O_pn₄} cells with a $K_d = 0.28$ nM and $B_{\text{max}} = 2.9$ pmoles/mg protein. Specific binding was 94% at 300 pM of radio ligand. **(b)** Concentration-dependent displacement of radio ligand by 9-*cis* retinal, AA92593 and AA41612. **(c)** Schild plot demonstrating competitive interaction between retinal and opsinamide. Peak light-induced Ca^{2+} fluorescence from CHO^{O_pn₄} cells incubated with buffer or different concentrations of AA92593 followed by increasing concentrations of 9-*cis* retinal are shown. Notice the rightward shift of retinal concentration curves reflecting increasing amount of retinal required to outcompete higher amount of opsinamide. The suppression of peak response with the highest concentrations of antagonist were caused by non-equilibrium conditions in the FLIPR. **(d)** Schild regression

plot showing competitive binding between opsinamide and 9-*cis* retinal. This dose ratio plot has a slope of 0.9 whose deviation from a slope of 1 was not statistically significant. The Schild plot showed AA92593 has an apparent K_b of 105 nM for human melanopsin in this experiment. Untransfected CHO cells showed < 5% of the specific binding observed with CHO^{Opn4}.

Author Manuscript

Author Manuscript

Author Manuscript

Author Manuscript

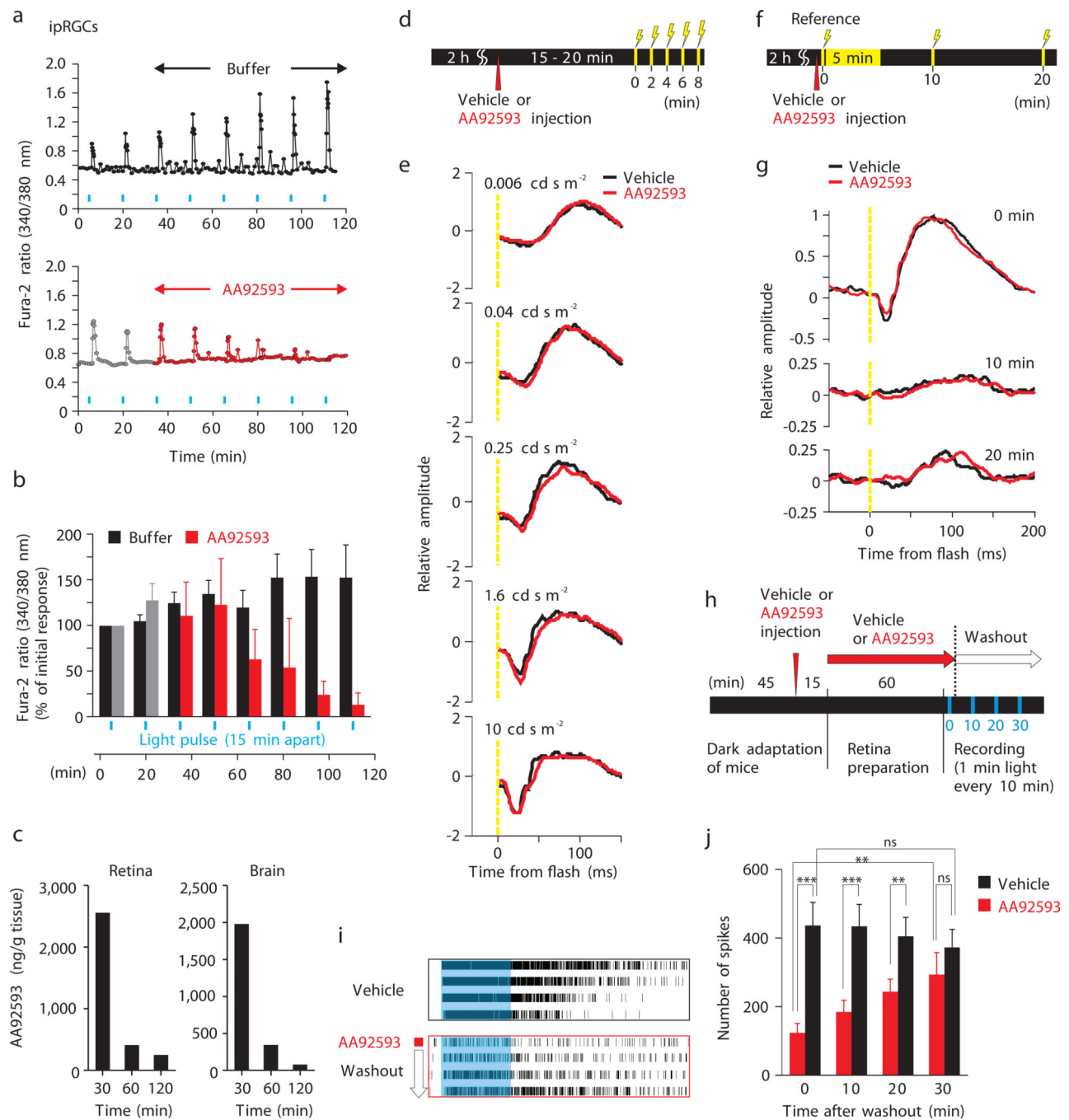


Fig. 3. Opsinamide inhibits melanopsin photoreponses without inhibiting rod/cone function. **(a)** Representative and **(b)** average (\pm SEM) light-evoked rise in Ca^{2+} in individual rat ipRGCs superfused with buffer ($n = 14$) or $10 \mu\text{M}$ AA92593 ($n = 7$) in response to stimulation with 1 min light (blue bars). **(c)** Concentration of AA92593 in the retina and brain at different times after the mice were IP injected with $30 \text{ mg} \cdot \text{kg}^{-1}$ of the compound. **(d to g)** ERG of *Opn4*^{-/-} mice treated with vehicle or opsinamides. **(d and e)** Mice received either vehicle (black, $n = 6$) or AA92593 (red, $n = 8$) and after 15–20 min they were exposed to successive light

flashes (250 ms) of increasing intensity. **(f and g)** Immediately after receiving either vehicle (black. $n = 6$) or AA92593 (red. $n = 8$), the mice were given a reference light pulse (time 0, 5 cd s/m², 250 ms), and exposed to an intense illumination (500 cd s/m²) for 5 min to bleach rod/cone photoreceptor responses. Recovery response to light flashes (5 cd s/m², 250 ms) was assessed at 10 and 20 min. **(h)** Experimental design of MEA recording of light-evoked responses from rd retina. **(i)** Example spike train raster plots of single units responding to 4 consecutive light pulses. **(j)** Average (+ SEM, $n = 24-50$ units) number of spikes in response to 1 min light pulse at 0, 10, 20, and 30 min after washout (* $P < 0.05$, ** < 0.01 , *** < 0.001 , NS, Student's t test).

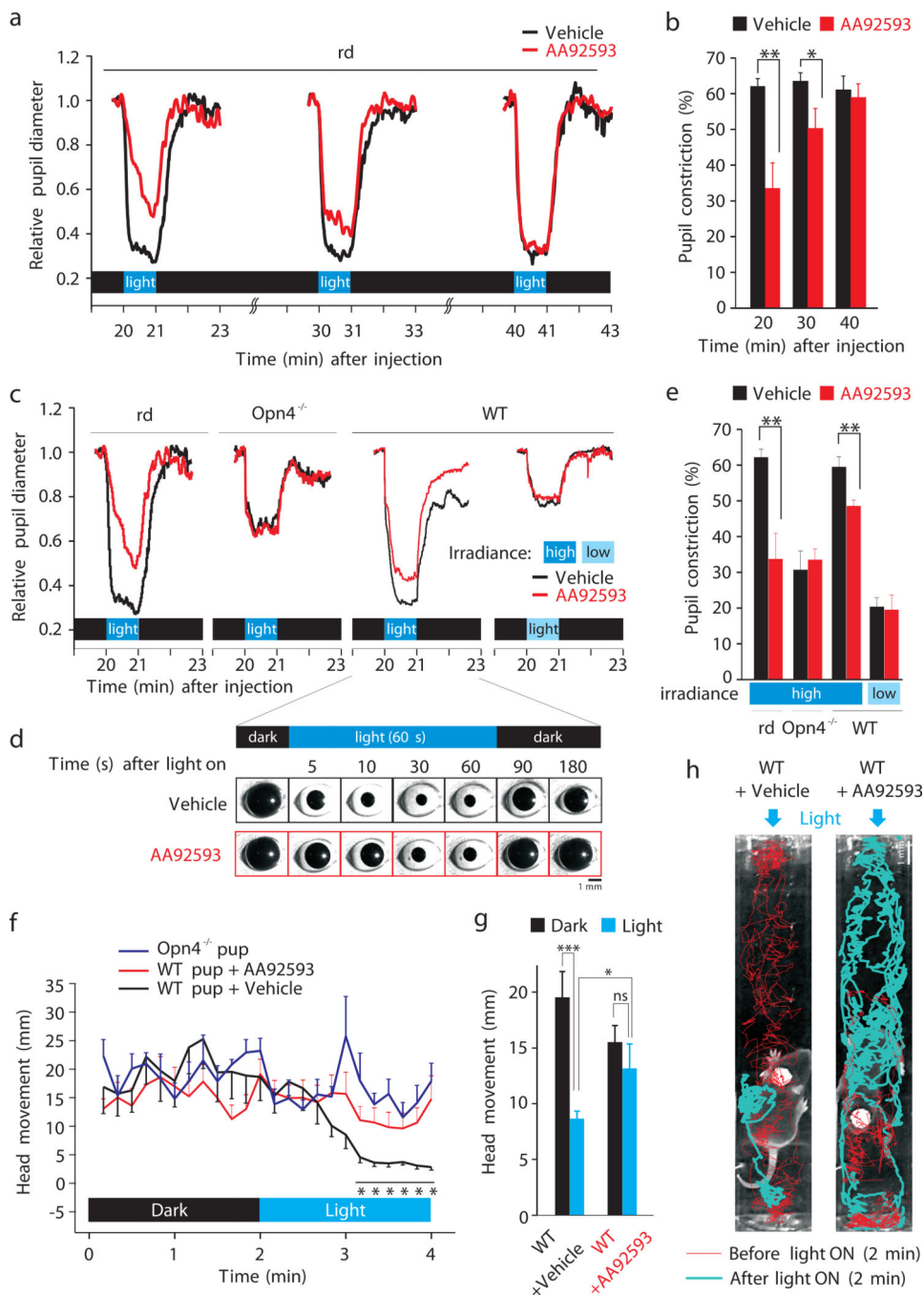


Fig. 4. Opsinamides reversibly attenuate melanopsin-mediated photoresponses. **(a)** Average pupil diameter in response to three individual light pulses. **(b)** Average pupil constriction (\pm SEM, $n = 6-7$) in vehicle- or opsinamide- treated mice. **(c)** Average pupil diameter of mice with melanopsin only (*rd*), rod/cone only (*Opn4*^{-/-}) or WT mice carrying both rod/cone and melanopsin photopigments in response to high or low irradiance levels. PLR for *rd* mice is reproduced from **a**. **(d)** Representative pictures of the eye of a WT mouse, showing the differences in pupil constriction after injection of vehicle or opsinamide. **(e)** Average

(+SEM, $n = 6$) pupil diameter during a 1 min light pulse in mice shown in **c**. **(f)** AA92593 attenuates phototaxis behavior in WT neonatal mice. Binned average (\pm SEM, $n = 10$ for WT + vehicle, $n = 12$ for WT + AA92593, $n = 7$ for *Opn4*^{-/-}, 10 s bins) head movement under darkness and after illumination showed significantly reduced ($*P < 0.05$, Student's *t* test) light aversion and freezing in WT pups treated with AA92593 that is similar to head movement in *Opn4*^{-/-} pups. **(g)** Average head movement (\pm SEM) over 2 min period in dark and after light are shown ($***P < 0.0005$, $*P < 0.05$). **(h)** Representative infrared images of WT littermate P8-aged pups injected with vehicle or AA92593 in a test chamber. Red and blue lines track the head movement of the mouse during 2 min prior to and 2 min after illumination with blue light, respectively. Arrows indicate the orientation of light after 2 min of baseline recording. Their activities are also shown in Supplementary Fig. 10 and Supplementary movies.